JMEPEG (2007) 16:12–21
DOI: 10.1007/s11665-006-9002-2

1059-9495/$19.00

Dendritic Growth in an Aluminum-Silicon Alloy

H. Kaya, E. Çadırlı, and M. Gündüz

(Submitted December 16, 2005; in revised form May 8, 2006)

Unidirectional solidification experiments have been carried out on an Al-3 wt.% Si alloy as a function of temperature gradient, *G* and growth rate, *V*. The samples were solidified under steady-state conditions with a constant growth rate of 8.20 μm/s at different temperature gradients (1.97-6.84 K/mm) and with a constant temperature gradient (6.84 K/mm) at different growth rates (8.20-492.76 μm/s). Microstructure parameters (primary dendrite arm spacing, λ_1, secondary dendrite arm spacing, λ_2, dendrite tip radius, *R* and mushy zone depth, *d*) were measured as a function of temperature gradient and growth rate. The experimental results have been compared with the current theoretical models and similar experimental works.

Keywords Al-Si alloy, directional solidification, dendritic growth, microstructures

1. Introduction

Aluminum alloys with silicon as a major alloying element are a class of alloys, which are the basis of many manufactured castings. This is mainly due to the outstanding effect of silicon in the improvement of casting characteristics, combined with other physical properties, such as mechanical properties and corrosion resistance (Ref 1). The microstructure formation during solidification depends on the alloy characteristics and primarily is a function of the temperature profiles at the solidification interface. When a metallic alloy is solidified, the most frequently observed solid morphology is the dendritic microstructure (Ref 2). In the dendritic solidification of alloys, the solute redistributes due to the difference in solubility between the liquid and solid phases. The solute rejected from the solid-liquid interface develops a region in the liquid in which the actual temperature is lower than the liquidus temperature and leads to constitutional supercooling (Ref 3). Dendritic microstructures are characterized by the microstructure parameters. Numerous solidification studies have been reported with a view to characterizing the microstructural parameters such as primary dendrite arm spacing (λ_1), secondary dendrite arm spacing (λ_2), dendrite tip radius (R) and mush zone depth (d) as a function temperature gradient (G) and growth rate (V) ahead of the microscopic solidification front (Ref 4-16).

A literature survey shows that several theoretical studies (Ref 6-10, 17-23) and theoretical models (Ref 20, 22, 24-31) have been used to examine the influence of solidification parameters (G, V) on microstructure parameters (λ_1, λ_2, R and d). According to these results an increase in the solidification parameters results in a decrease in microstructure parameters.

Theoretical models have been proposed in the literature to describe λ_1 as a function of V, G and C_o by Hunt (Ref 24), Kurz and Fisher (Ref 25), Trivedi (Ref 26), Hunt and Lu (Ref 20) and Bouchard and Kirkaldy (Ref 27, 28). Hunt allowed for the interaction of the diffusion fields between neighboring cells. The relationship between λ_1 and solidification parameters (G, V, C_o) for a spherical dendritic front with the growth condition for dendrites is determined by the minimum undercooling. Equation (1) presents the Hunt model,

$$\lambda_1 = 2.83[m\ (k-1)D\Gamma]^{0.25}\ C_o^{0.25} V^{-0.25} G^{-0.5} \qquad \text{(Eq 1)}$$

where m is liquidus slope, k is partition coefficient, D is diffusion coefficient in liquid and Γ is Gibbs-Thomson coefficient.

Another theoretical model to characterize λ_1 as function of G, V and C_o was developed by Kurz and Fisher (Ref 25). They assumed that the shape of the cell or dendrite can be approximated as ellipsoids and using the marginal stability criterion for an isolated dendrite or cell, they simplified their results for the low velocity ($V < V_{cs}/k$) and for the high velocity ($V > V_{cs}/k$) regimes (where V_{cs} is the critical velocity at which the planar interface becomes unstable). For $V > V_{cs}/k$, Kurz and Fisher obtained,

$$\lambda_1 = 4.3\left[m(k-1)D\Gamma/k^2\right]^{0.25} C_o^{0.25} V^{-0.25} G^{-0.5} \qquad \text{(Eq 2)}$$

Another theoretical model to characterize λ_1 as function of G, V, C_o was developed by Trivedi (Ref 26). Trivedi modified the Hunt model by inserting marginal stability criterion. Equation (3) presents the Trivedi model,

$$\lambda_1 = 2.83[m(k-1)D\Gamma L]^{0.25} C_o^{0.25} V^{-0.25} G^{-0.5} \qquad \text{(Eq 3)}$$

where L is a constant depending on harmonic perturbations. According to Trivedi, for dendritic growth, L can be any value between 10 and 28. These theoretical models are very similar at high growth rate for λ_1 and the difference among them is only a constant.

H. Kaya and **E. Çadırlı**, Department of Physics, Faculty of Arts and Sciences, Niğde University, Niğde, Turkey; and **M. Gündüz**, Department of Physics, Faculty of Arts and Sciences, Erciyes University, Kayseri, Turkey; Contact e-mail: hkaya@nigde.edu.tr.

Hunt and Lu (Ref 20) investigated the cellular/dendritic array growth by using a numerical model. They presented analytic expressions that fitted with the numerical results. According to the Hunt and Lu model, in the absence of convection, the dimensionless primary dendrite arm spacing is given by,

$$\lambda' = 0.07798 V'^{(a-0.75)}(V' - G')^{0.75} G'^{-0.6028} \quad \text{(Eq 4)}$$

where, $\lambda' = \lambda \Delta T_o/(\Gamma k)$, $G' = G\Gamma k/(\Delta T_o)^2$, $V' = V\Gamma k/(D\Delta T_o)$, $\Delta T_o = mC_o(k-1)/k$ and $a = -1.131 - 0.1555 \log G' - 0.007589 (\log G')^2$ where λ', G' and V' are dimensionless parameters.

Another theoretical model was proposed by Bouchard and Kirkaldy (Ref 27, 28). These authors calculated the primary dendrite spacings and assumed the solidification under the conditions of unsteady-state heat flow.

$$\lambda_1 = a_1 \left(\frac{16\, C_o^{1/2} G_o \varepsilon \Gamma D}{(1-k) m G V} \right)^{1/2} \quad \text{(Eq 5)}$$

where $G_o\varepsilon$ is a characteristic parameter $\approx 600 \times 6$ K $\cdot$ (cm)$^{-1}$, a_1 is the primary dendrite-calibrating factor, which depends on the alloy composition (see Appendix A).

Langer and Müller-Krumbhaar (Ref 22) carried out a detailed numerical analysis of the wavelength of instabilities along the sides of a dendrite and predicted the scaling law as $\lambda_2/R = 2$. Using the scaling law $\lambda_2/R = 2$, the variation in λ_2 for small peclet number conditions given by Trivedi and Somboonsuk (Ref 29) was obtained as,

$$\lambda_2 = (8\Gamma DL/kV\Delta T_o)^{0.5} \quad \text{(Eq 6)}$$

where ΔT_o is the difference between the liquidus and solidus equilibrium temperatures.

For secondary dendrite spacings, Bouchard and Kirkaldy (Ref 27, 28) derived an expression, which is very similar to the marginal wavelength formula (Ref 7).

$$\lambda_2 = 2\pi a_2 \left(\frac{4\Gamma}{C_o (1-k)^2 T_F} \left(\frac{D}{V} \right)^2 \right)^{1/3} \quad \text{(Eq 7)}$$

where a_2 is the secondary dendrite-calibrating factor, which depends on the alloy composition (see Appendix A) and T_F is the fusion temperature of the solvent.

As mentioned above, the Hunt (Ref 24), the Kurz-Fisher (Ref 25) and the Trivedi (Ref 26) models were used to find the relationships between R as a function V and C_o. R is given

$$R = [2\Gamma D/m(k-1)]^{0.5} C_o^{-0.5} V^{-0.5} \quad \text{(Eq 8)}$$

$$R = 2\pi[\Gamma D/m(k-1)]^{0.5} C_o^{-0.5} V^{-0.5} \quad \text{(Eq 9)}$$

$$R = [2k\Gamma DL/m(k-1)]^{0.5} C_o^{-0.5} V^{-0.5} \quad \text{(Eq 10)}$$

in Hunt model (Ref 24), Kurz and Fisher model (Ref 25) and Trivedi model (Ref 26), respectively (Eq 8-10). As can be seen from Eq (8-10) the theoretical models for R are also very similar and the difference among them is only a constant.

Rutter and Chalmers (Ref 30) and Tiller et al. (Ref 31) derived mushy zone depth formula from the constitutional supercooling criterion in the absence of convection.

$$d = \frac{\Delta T_o}{G} \quad (\Delta T_o = -m\Delta C_o = T_L - T_S) \quad \text{(Eq 11)}$$

where T_L and T_s are liquidus and solidus temperature of the solvent, respectively.

The aim of the present work was to experimentally investigate the dependency of the λ_1, λ_2, R and d on G and V in the directionally solidified Al-3 wt.% Si binary alloy system and to compare the results with the current theoretical models (Ref 20, 22, 24-31) and previous experimental results (Ref 5, 11-16, 32-63).

2. Experimental Procedure

The Al-3 wt.% Si alloy samples were prepared by melting weighed quantities of Al and Si of >99.9% purity in a graphite crucible placed into a vacuum melting furnace (Ref 54). After allowing time for melt to become homogeneous, the molten alloy was poured into 13 graphite crucibles (250 mm in length 4 mm ID and 6.35 mm OD) in a hot filling furnace (Ref 55). Each specimen was than positioned in a Bridgman-type furnace (Fig. 1 and 2) in a graphite cylinder (300 mm in length 10 mm ID and 40 mm OD). After stabilizing the thermal conditions in the furnace under an argon atmosphere, the specimen was grown by pulling downwards at a constant rate by means of a synchronous motor. Samples were solidified under steady-state conditions with a constant growth rate (8.20 μm/s) and different temperature gradients (1.97-6.84 K/mm), and with a constant temperature gradient (6.84 K/mm) and different growth rates (8.20-492.76 μm/s) as shown in Table 1. After 80-120 mm steady-state growth of the samples, they were quenched by pulling them rapidly into the water reservoir.

2.1 The Measurement of Temperature Gradient, G and Growth Rates, V

The temperature of the Bridgman-type furnace was controlled by a Pt/Pt-13%Rh thermocouple placed between the heating element and the alumina tube. The temperature can be controlled to about ±0.1 K during the run. The thermocouples were placed into capillary alumina tubes (0.8 mm ID, 1.2 mm OD) which were positioned approximately 10 mm apart and parallel to the heat flow direction inside the crucible (Fig. 2). Throughout the experiment, temperature distribution was obtained by measuring the temperature in the sample by three chromel/alumel thermocouples (K-type), which were placed in the sample. All the thermocouple outputs were taken to data-logger and computer (Fig. 1).

Signals from three thermocouples were recorded simultaneously by means of a data-logger to measure the temperature gradients at the solid/liquid interface in the liquid. When the second thermocouple was at the solid-liquid interface and the third thermocouple in the liquid, their temperatures were used to obtain the temperature gradient, G. G can be kept constant during the run by keeping constant the temperature of the

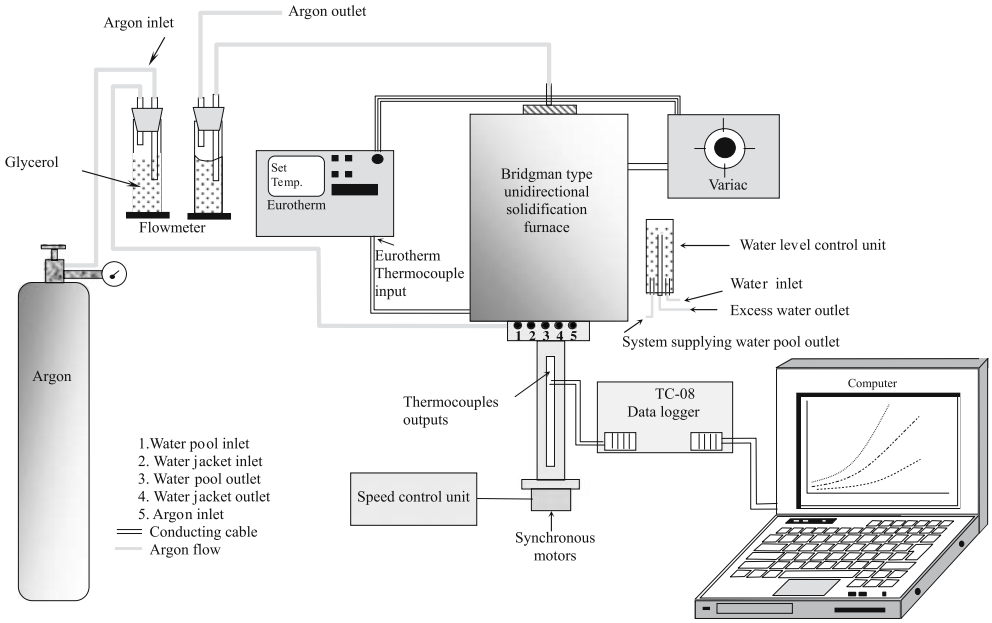

Fig. 1 The Bridgman-type directional solidification experimental system and equipments

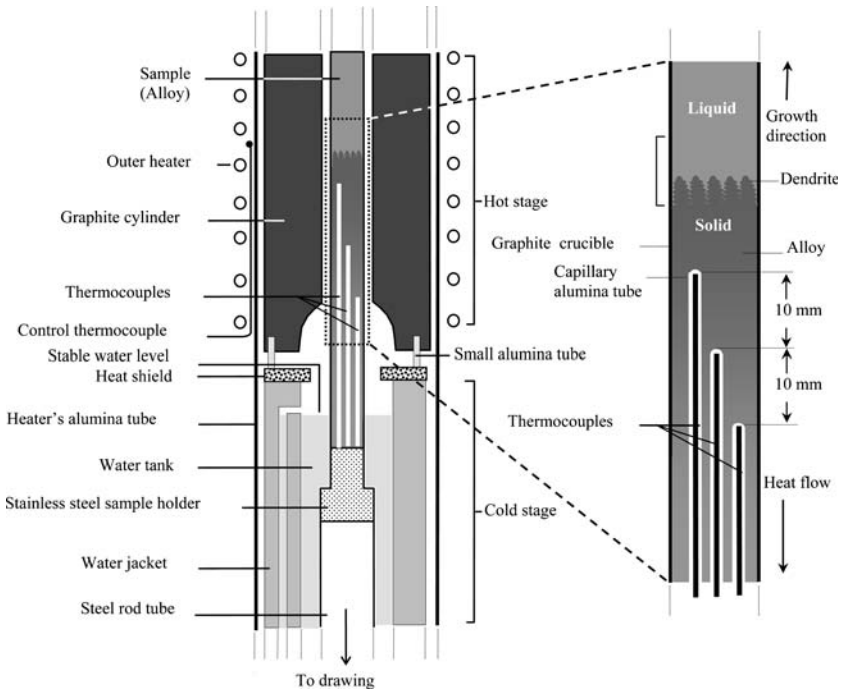

Fig. 2 The details of the Bridgman-type directional solidification furnace, (a) Hot and cold stages of the furnace, (b) the sample

cooler and the hotter part of the furnace, and the distance between them.

The growth rate was calculated through two different methods. In the first method, the values for the growth rate were calculated from the measurements of the time taken for the solid/liquid interface to pass the thermocouples separated by a known distance. In the second method, the total solidification time and solidification distance (on the longitudinal section of the polished sample) were measured. The ratio of the distances to the times gives the growth rates, and these were similar in both methods.

2.2 Metallographic Examination

The directionally solidified and quenched specimen was removed from the graphite crucible and then ground to observe the solid-liquid interface. The longitudinal section, which included the quenched interface was separated from the

Table 1 Microstructure parameters (λ_1, λ_2, R and d) for the directionally solidified Al-3 wt.% Si alloy and the experimental relationships

G, K/mm	V, μm/s	$\lambda_{1(tr)}$, μm	$\lambda_{1(ar)}$, μm	$\lambda_{1(ave)}$, μm	λ_2, μm	R, μm	d, μm	λ_2/R
1.97	8.2	827 ± 81	793 ± 80	810 ± 80	89 ± 7.0	44 ± 3.5	2400 ± 209	2.02
3.1	8.2	734 ± 62	706 ± 59	720 ± 62	76 ± 6.2	36 ± 2.9	1950 ± 186	2.11
4.25	8.2	620 ± 46	600 ± 44	610 ± 60	65 ± 4.0	31 ± 2.8	1300 ± 136	2.09
5.56	8.2	544 ± 55	516 ± 52	530 ± 56	53 ± 5.3	27 ± 2.0	1030 ± 88	1.96
6.84	8.2	465 ± 40	455 ± 37	460 ± 39	42 ± 2.4	20 ± 1.9	825 ± 80	2.1
6.84	16.52	377 ± 36	363 ± 34	370 ± 36	34 ± 2.8	16 ± 1.6	664 ± 56	2.1
6.84	41.53	325 ± 29	315 ± 28	320 ± 32	25 ± 1.5	11 ± 1.5	440 ± 32	2.13
6.84	82.42	260 ± 24	246 ± 23	253 ± 27	19 ± 1.6	8.2 ± 0.8	330 ± 45	1.92
6.84	163.6	196 ± 22	194 ± 19	195 ± 20	12 ± 1.1	5.8 ± 1.1	250 ± 28	2.11
6.84	492.76	146 ± 11	144 ± 13	145 ± 13	6.4 ± 0.8	3.3 ± 0.6	190 ± 16	2.33
Experimental relationships (constant V)		$\lambda_{1(tr)} = k_1 G^{-0.47}$	$\lambda_{1(ar)} = k_2 G^{-0.46}$	$\lambda_{1(ave)} = k_3 G^{-0.47}$	$\lambda_2 = k_4 G^{-0.58}$	$R = k_5 G^{-0.59}$	$d = k_6 G^{-0.89}$	$\lambda_2/R_{ave} = 2.09$
Experimental relationships (constant G)		$\lambda_{1(tr)} = k_7 V^{-0.28}$	$\lambda_{1(ar)} = k_8 V^{-0.27}$	$\lambda_{1(ave)} = k_9 V^{-0.28}$	$\lambda_2 = k_{10} V^{-0.47}$	$R = k_{11} V^{-0.45}$	$d = k_{12} V^{-0.38}$	
Regression constant (k)			Correlation coefficient (r)					
$k_1 = 49.09$ ($\mu m^{0.53} \cdot K^{0.47}$)			$r_1 = -0.983$					
$k_2 = 49.44$ ($\mu m^{0.54} \cdot K^{0.46}$)			$r_2 = -0.985$					
$k_3 = 1166.8$ ($\mu m^{0.53} \cdot K^{0.47}$)			$r_3 = -0.991$					
$k_4 = 140.9$ ($\mu m^{0.42} \cdot K^{0.58}$)			$r_4 = -0.972$					
$k_5 = 73.28$ ($\mu m^{0.41} \cdot K^{0.59}$)			$r_5 = -0.969$					
$k_6 = 4677.0$ ($\mu m^{0.11} \cdot K^{0.89}$)			$r_6 = -0.986$					
$k_7 = 866.96$ ($\mu m^{1.28} \cdot sn^{-0.28}$)			$r_7 = -0.993$					
$k_8 = 812.93$ ($\mu m^{1.27} \cdot sn^{-0.27}$)			$r_8 = -0.995$					
$k_9 = 851.14$ ($\mu m^{1.28} \cdot sn^{-0.28}$)			$r_9 = -0.994$					
$k_{10} = 124.17$ ($\mu m^{1.47} \cdot sn^{-0.47}$)			$r_{10} = -0.989$					
$k_{11} = 54.95$ ($\mu m^{1.45} \cdot sn^{-0.45}$)			$r_{11} = -0.996$					
$k_{12} = 1819.7$ ($\mu m^{1.38} \cdot sn^{-0.38}$)			$r_{12} = -0.999$					

$\lambda_{1(tr)}$: The values of the primary dendrite arm spacing obtained from the transverse section using the triangle method
$\lambda_{1(ar)}$: The values of the primary dendrite arm spacing obtained from the transverse section using the area counting method
$\lambda_{1(ave)}$: Average values of λ_{tr} and λ_{ar}

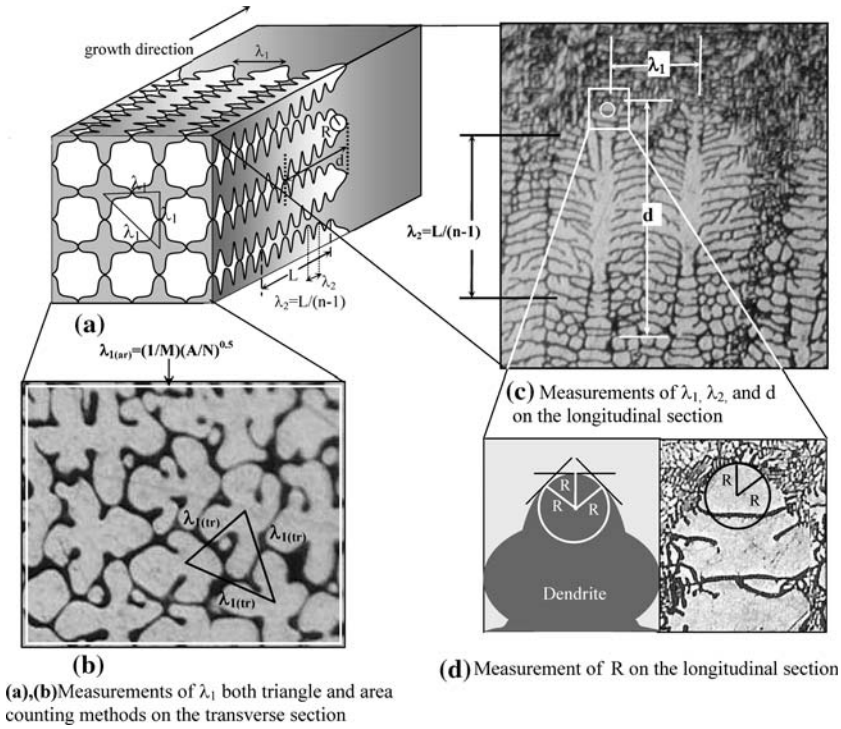

Fig. 3 The schematic and photographic illustration of dendritic structures

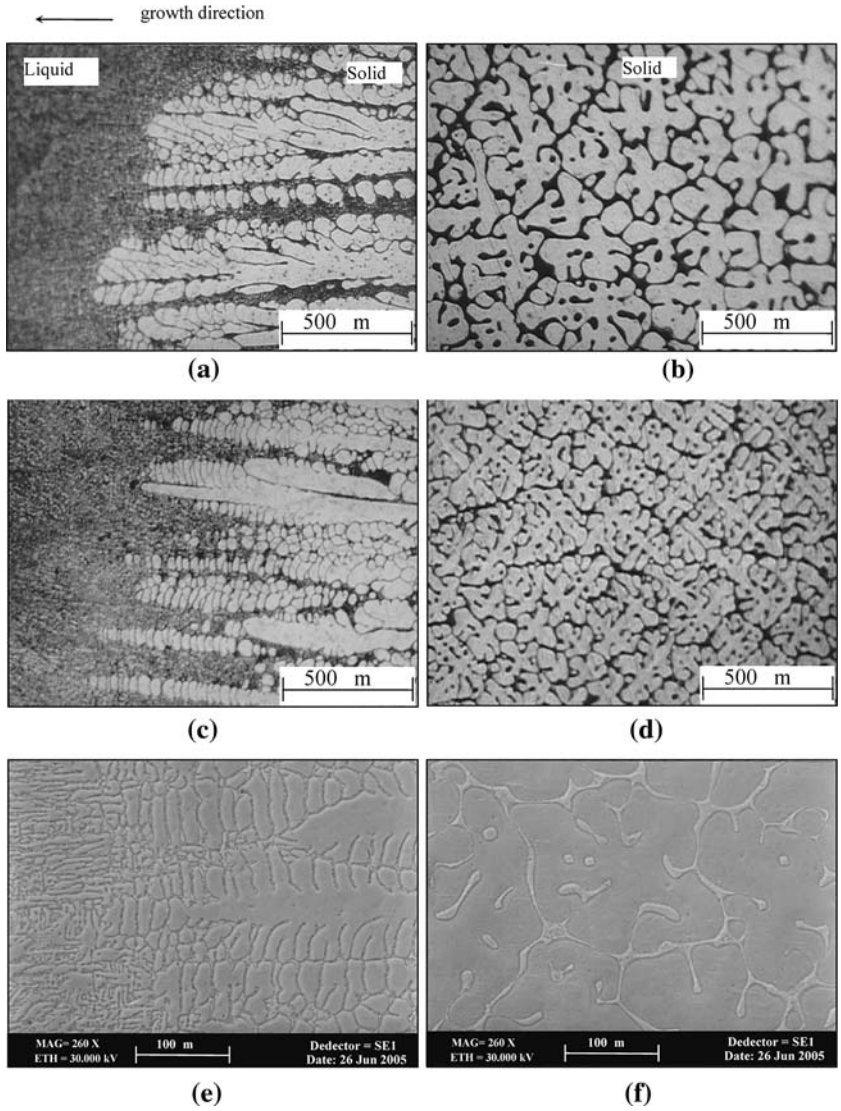

Fig. 4 Solidification microstructures of Al-3 wt.% Si alloy (a) longitudinal (b) transverse sections for G = 4.25 K/mm, V = 8.2 μm/s, (c) longitudinal (d) transverse sections for G = 6.84 K/mm, V = 16.5 μm/s, (e) longitudinal (f) transverse sections for G = 6.84 K/mm, V = 492.8 μm/s (SEM)

specimen. Thereafter, transverse and longitudinal sections of the specimens were cut from the samples and cold-mounted in epoxy-resin. The samples were wet ground down to grit 2500 and mechanically polished using 6, 3, 1 and 1/4 μm diamond paste. Finally the specimens were etched with an acid solution (100 mL H_2O and 4 mL HF) to reveal the microstructure.

The microstructures of the specimen were investigated under an optical microscope (Olympus, BH-2) and a scanning electron microscopy (SEM, LEO-l model) (Fig. 3 and 4).

2.3 Measurements of Microstructure Parameters (λ_1, λ_2, R, d)

The primary dendrite arm spacing λ_1 was obtained by measuring the distance between the nearest two dendrites tips. λ_1 was measured on the transverse section (perpendicular to the growth direction). Figure 3(a) and (b) and Fig. 4(b), (d) and (f) give more accurate results than the λ_1 values measured on the longitudinal section (parallel to the growth direction). Two different methods were used to measure the primary dendrite arm spacings on the transverse sections. The first method is the triangle method (Ref 56). The triangle is formed by joining the three neighboring dendrite centers, and sides of the triangle corresponded to $\lambda_{1(tr)}$ (see Fig. 3). The second method is the area counting method (Ref 33, 55-57). In this method, $\lambda_{1(ar)}$ values were measured on the cross-section, at least in four different regions of each specimen (see Fig. 3). $\lambda_{1(ar)}$ is equal to $(1/M)(A/N)^{0.5}$ where M is the magnification factor, A is the total specimen cross-sectional area and N is the number of primary dendrites on the cross-section. λ_2 values were measured by averaging the distance between adjacent side branches on the longitudinal section of a primary dendrite. Each of side-branch spacing data reported here is the average of the initial λ_2 values from 5 to 10 primary dendrites for each specimen. R was measured by fitting a suitable circle on the dendrite tip side. d is defined by the distance between tip side and root side of the

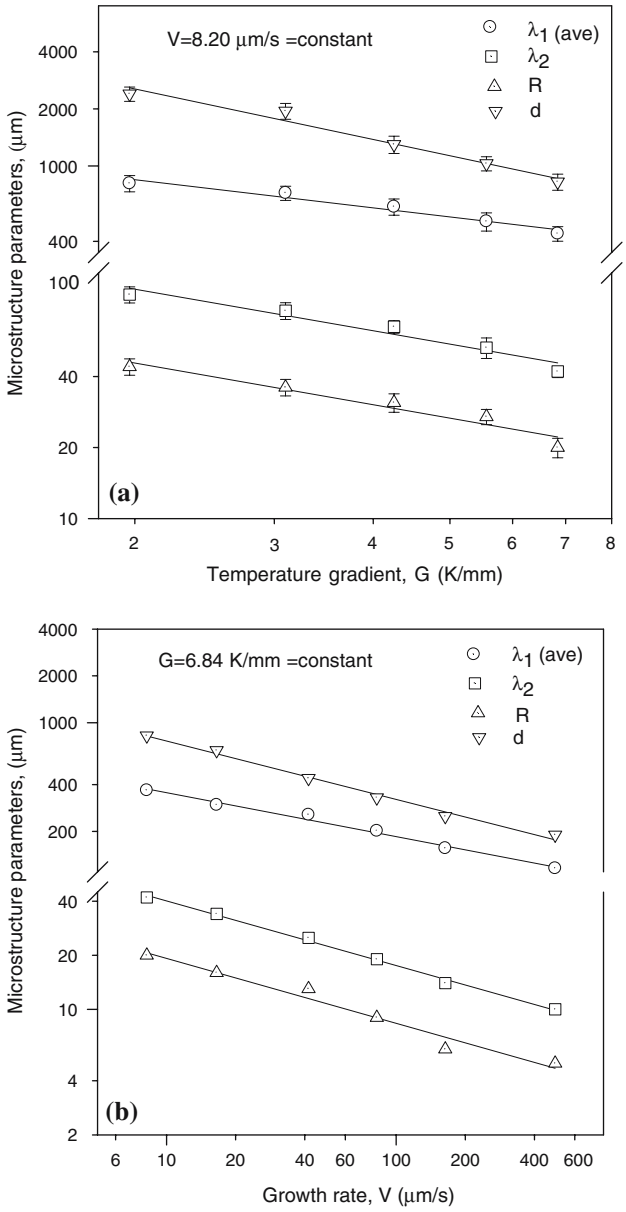

Fig. 5 Variation of microstructure parameters according to solidification parameters, (a) Variation of microstructure parameters as a function of G at the constant V = 8.20 μm/s. (b) Variation of microstructure parameters as a function of V at the constant G = 6.84 K/mm

dendrites (Fig. 3a, c and 4a, c, e). This parameter was measured as far from steady-state condition in the dendrites as possible, and taken to be the average value of these measurements.

In the measurements of λ_1, λ_2, R and d, 150-200 values for each G and V were measured to increase statistical sensitivity. Thus, the values of λ_1, λ_2, R and d were measured as a function of G and V for the Al-3 wt.% Si system.

3. Results and Discussion

Al-3 wt.% Si alloy was solidified with a constant V at different G and with a constant G at different V, and typical microstructures of this alloy are shown in Fig. 4. The dependency of the λ_1, λ_2, R and d on G and V was calculated by a linear regression analysis. These calculations have led to the establishment of the following general relationships;

$$(\lambda_1, \lambda_2, R, d) = k_i G^{-a_i}$$

$$(\lambda_1, \lambda_2, R, d) = k_i V^{-b_i}$$

where k_i are various proportionality constants, and a_i and b_i are various temperature gradient and the growth rate exponent values, respectively. Experimental observations show that the values of λ_1, λ_2, R and d decrease as G and V increase. The relationships between microstructure parameters (λ_1, λ_2, R and d) and the solidification parameters (G and V) with a constant C_o composition have been obtained to be $\lambda_{1(ave)} = k_3 G^{-0.47}$, $\lambda_2 = k_4 G^{-0.58}$, $R = k_5 G^{-0.59}$, $d = k_6 G^{-0.89}$ and $\lambda_{1(ave)} = k_9 V^{-0.28}$, $\lambda_2 = k_{10} V^{-0.47}$, $R = k_{11} V^{-0.45}$, $d = k_{12} V^{-0.38}$.

As can be seen from Table 1 and Fig. 5, the values of λ_1, λ_2, R and d decrease as G increase at a constant V. The average exponent values of λ_1, λ_2, R and d in Al-3 wt.% Si alloy for different G and constant V were found to be −0.47, −0.58, −0.59 and −0.89, respectively. The values of λ_1, λ_2, R and d decrease as V increases at a constant G. The average exponent values of λ_1, λ_2, R and d for different V and constant G were found to be −0.28, −0.47, −0.45 and −0.38, respectively. These relationships show that the dependency of the λ_1, λ_2, R and d on G are stronger than on V.

The exponent values of λ_1, λ_2, R and d for Al-3 wt.% Si alloy obtained in the present work are for the most part in good agreement with the exponent values of λ_1, λ_2, R and d obtained in previous works (Ref 5, 11-16, 32-53) for different alloy systems.

The comparisons of the experimentally obtained λ_1 values in present work with the calculated λ_1 values by the Hunt (Ref 24), the Kurz-Fisher (Ref 25), the Trivedi (Ref 26), the Hunt-Lu (Ref 20) and the Bouchard-Kirkaldy (Ref 27, 28) models are given in Fig. 6(a-d). The physical parameters of Al-3 wt.% Si alloy used in calculations for the values of λ_1, λ_2, R and d with the theoretical models are given in Appendix A. As can be seen from Fig. 6(a), the calculated values of λ_1 with the Trivedi (Ref 26) model agrees very well with our experimental values, but calculated values of λ_1 with the Kurz-Fisher (Ref 25) model gives higher value and the Hunt (Ref 24) model gives smaller value than our experimental values (for constant V and different G and constant G and different V).

It can be noted from Fig. 6(b) that the calculated value of λ_1 with Hunt-Lu (Ref 20) model gives smaller value than the experimental values at growth rates higher than 20 μm/s. On the other hand, the values of λ_1 are in good agreement with the experimental values at growth rates smaller than 20 μm/s. It can be seen from Fig. 6(c) that the calculated values of λ_1 with Bouchard-Kirkaldy (Ref 27, 28) model are in good agreement with our experimental results for a constant V (V = 8.2 μm/s) and different G (1.97-6.84 K/mm). As can be seen from Table 1, both theoretical temperature gradient exponent (0.50) and the experimental exponent (0.47) are very close to each other, but λ_1 values exhibit discrepancies from the experimental values for a constant G (6.84 K/mm) and different V (8.2-492.7 μm/s) (see Fig. 6d). As can be seen from Eq 5, this might be because of the theoretical exponent value of λ_1 is 0.50 for growth rate (V) but experimentally obtained exponent value of V is 0.28. Although, the Hunt (Ref 24), the Kurz-Fisher (Ref 25) and the

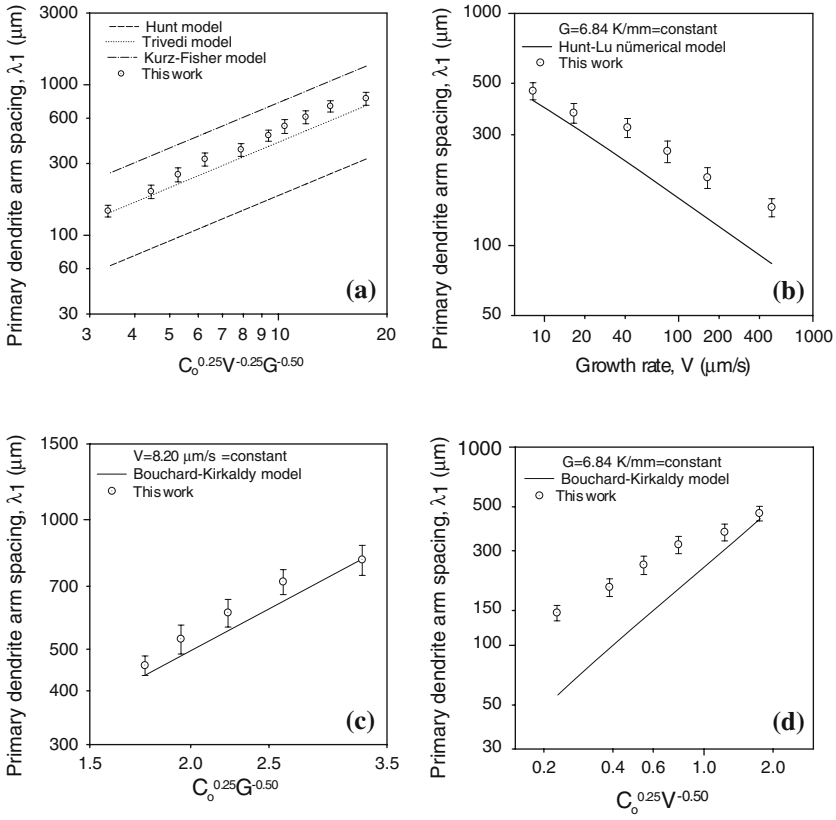

Fig. 6 Comparison of experimental and theoretical λ_1 values as a function of V and G for Al-3 wt.% Si alloy

Trivedi (Ref 26) models leads to a theoretical exponent value of 0.25 for the growth rate, Bouchard-Kirkaldy (Ref 27, 28) model leads to a theoretical exponent value of 0.5 for the growth rate.

In the present work, the λ_2 values experimentally obtained as a function of growth rate have been compared with the values of λ_2 calculated from the Trivedi-Somboonsuk (Ref 29) and the Bouchard-Kirkaldy (Ref 27, 28) models, and the comparisons are given in Fig. 7(a) and (b), respectively. As can be seen from Fig. 7(a), the calculated values of λ_2 from the Trivedi-Somboonsuk (Ref 29) model as a function of $(C_oV)^{-0.5}$ agree very well with our experimental values. In contrast, Fig. 7(b) shows that the calculated values of λ_2 with the Bouchard-Kirkaldy (Ref 27, 28) model as a function of $C_o^{-0.33}V^{-0.67}$ do not agree with our experimental values. This might be due to the different exponent value of the growth rates for the theoretical model (0.67) and the experimental work (0.47).

There is a clear difference between the exponent values obtained in the Trivedi-Somboonsuk (Ref 29) and the Bouchard-Kirkaldy (Ref 27, 28) models. Briefly, the theoretical Bouchard-Kirkaldy (Ref 27, 28) model, relating primary and secondary dendrite spacings with growth rate, has not agreed with the experimental resuts.

Figure 8(a) shows the comparisons of the experimentally obtained R values as a function of $(C_oV)^{-0.5}$ in a constant G with the values of R calculated from the Hunt (Ref 24), the Kurz-Fisher (Ref 25) and the Trivedi (Ref 26) models. It can be seen from Fig. 8(a) that the calculated values of R based on the the Kurz-Fisher (Ref 25) and the Trivedi (Ref 26) models are in good agreement with our experimental values. The values of R calculated with the Hunt (Ref 24) model are slightly smaller than our experimental values.

The results of the constitutional supercooling criterion (Ref 30, 31) calculated from Eq 11 are compared with the experimentally measured d values in Fig. 8(b). As can be seen from Fig. 8(b), the experimental results for the d values are slightly smaller than the predicted d values by the constitutional supercooling criterion (Eq 11).

The values of λ_2/R for Al-3 wt.% Si alloy are also given in Table 1, and the average value of λ_2/R is found to be 2.09. The value of λ_2/R for undercooled dendrites was estimated to be 2.1 for pure substances by Langer and Müller-Krumbhaar (Ref 22). Thus, the average value of λ_2/R obtained in the present work for Al-3 wt.% Si alloys is approximately equal to the value of λ_2/R estimated by Langer and Müller-Krumbhaar (Ref 22) for pure substances. In addition, the experimental value (2.09) is also very close to 2.0, 2.08, 2.8 and 2.8 values reported by Trivedi and Somboonsuk (Ref 29) for Succinonitrile-Acetone, and Kaya et al. (Ref 16) for Succinonitrile-CBr_4, Gündüz and Çadırlı (Ref 15) for Al-Cu alloys, and Liu et al. (Ref 61) for Succinonitrile-5.6 wt.% H_2O alloys, respectively. But, the experimental values are quite different from some of the other experimental results (Ref 12, 13, 58-60, 62, 63) (see Table 2).

4. Conclusions

In Al-3 wt.% Si alloy was directionally solidified under two sets of growth conditions: constant V (8.20 μm/s) and variable G (1.97-6.84 K/mm) and constant G (6.84 K/mm) and variable V (8.20-492.76 μm/s). Their microstructural features of

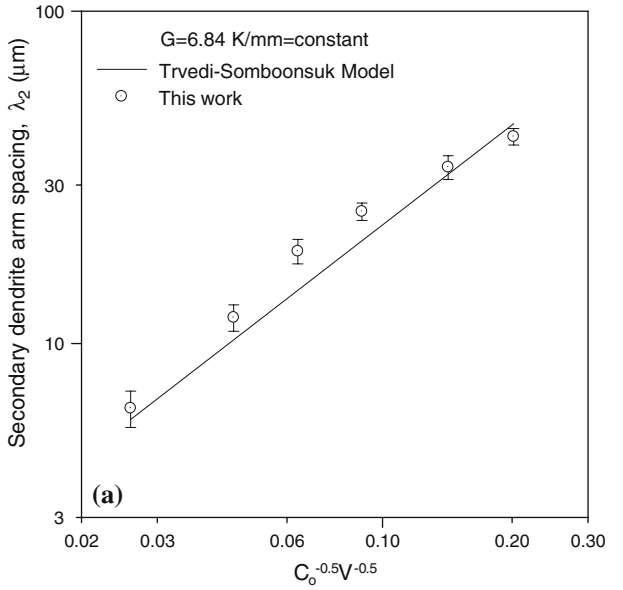

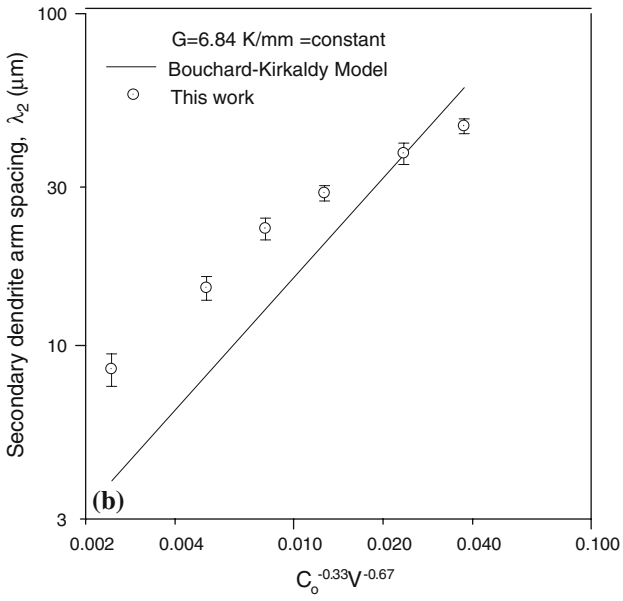

Fig. 7 Comparison of experimental and theoretical λ_2 values (a) secondary dendtrite arm spacing, λ_2 as a function of $V^{-0.5}$ (b) secondary dendtrite arm spacing, λ_2 as a function of $V^{-0.67}$

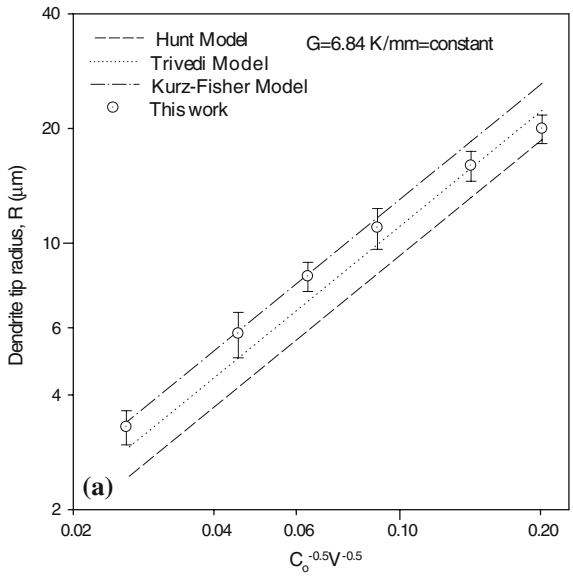

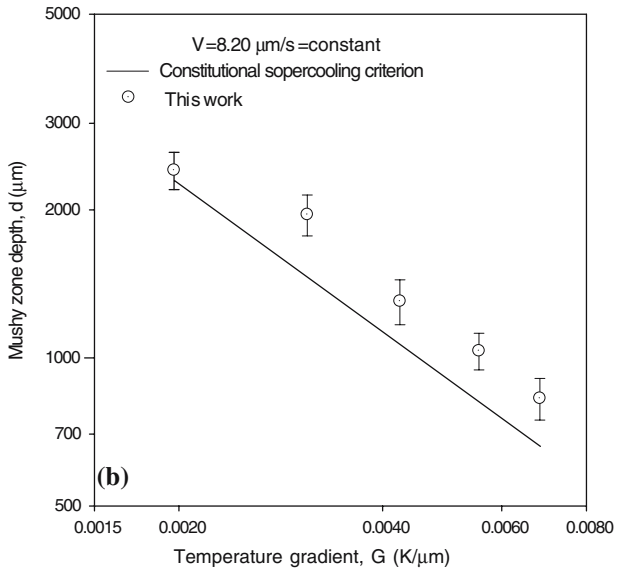

Fig. 8 (a) Comparison of the experimental and the theoretical denrite tip radius R values (R as a function of$(C_oV)^{-0.5}$) (b) Comparison of the experimental and the theoretical mushy zone depth d values (d as a function of G)

the grown samples were observed on the longitudinal and transverse sections of the specimen to examine the influence of the solidification parameters (G, V) on the microstructural parameters (λ_1, λ_2, R, d). It was found that the microstructure parameters (λ_1, λ_2, R, d) decrease as the solidification parameters (G, V) increase.

Some of the conclusions derived from the present work are as follows:

1. The values of λ_1 calculated from the Trivedi (Ref 26) model agree very well with the experimental λ_1 values, but calculated values of λ_1 from the Kurz-Fisher (Ref 25) model are slightly higher, and from the Hunt (Ref 24) model are significantly smaller than the experimental λ_1 values, respectively. The calculated values of λ_1 with Hunt-Lu (Ref 20) model are smaller than the experimental values at growth rates higher than 20 μm/s, but the values of λ_1 are in good agreement with experimental values at the growth rates smaller than 20 μm/s. The calculated values of λ_1 with Bouchard-Kirkaldy (Ref 27, 28) model are in good agreement with the experimental λ_1 values for the case of constant V and variable G, but the λ_1 values are quite different than the experimental λ_1 values for the case of constant G and variable V.
2. The calculated λ_2 values are in very good agreement with experimental λ_2 values for the Trivedi-Somboonsuk (Ref 29) model, but the Bouchard-Kirkaldy (Ref 27, 28) model, relating λ_2 with V, does not agree with the experimental resuts.
3. The calculated values of R with the Kurz-Fisher (Ref 25) model and the Trivedi (Ref 26) models are in good agreement with the experimental R values in this work. The calculated

Table 2 The λ_2/R values for some metallic and organic systems in the literature

Systems	λ_2/R values	Ref.
-	2.10 (Theoretical value)	(Ref 22)
Al-3 wt.% Si	2.09	This work
PVA	4.64	(Ref 12)
CAMP	3.33	(Ref 13)
Al-(3, 6, 15, 24) wt.% Cu	2.8	(Ref 15)
SCN-(5, 10, 20, 40) wt.% CTB	2.08	(Ref 16)
SCN-ACE	2.0	(Ref 29)
SCN	2.5	(Ref 47)
CBr_4-10.5 wt.% C_2Cl_6	3.18	(Ref 58)
CBr_4-7.9 wt.% C_2Cl_6	3.47	(Ref 58)
PVA-0.82 wt.% ETH	3.8	(Ref 59)
H_2O-NH_4Cl	4.68	(Ref 60)
SCN-5.6 wt.% H_2O	2.8	(Ref 61)
NH_4Cl-70 wt.% H_2O	4.02	(Ref 62)
SCN	3.0	(Ref 63)

SCN, Succinonitrile; PVA, Pivalic acid; CAMP, Camphene; ACE, Acetone; ETA, Ethanole; CTB(CBr_4), Carbon tetrabromüre

values of R with the Hunt (Ref 24) model is slightly lower than our experimental values.

4. The experimental values of d are slightly higher than the d values calculated from the constitutional supercooling criterion.
5. The λ_2/R value obtained in this work is in good agreement with both the theoretical value (2.10) (Ref 22) and values obtained by Trivedi-Somboonsuk (Ref 29), Liu and Hellawell (Ref 61), Gündüz and Çadırlı (Ref 15) and Kaya et al. (Ref 16). The λ_2/R values obtained in some organic systems (Ref 58-60, 62) are however, higher than our experimental results.

Appendix A

The physical constants for Al-3 wt.% Si alloy. Physical properties of Al-3 wt.% Si alloy used in the calculations

Liquidus slope (m)	2.25 (K/wt.%)	(Ref 64)
Diffusion coefficient in the liquid (D)	4300 $\mu m^2/s$	(Ref 65)
Equilibrium partition coefficient (k)	0.13	(Ref 64)
The Gibbs-Thomson coefficient (Γ)	0.196 (K · lm)	(Ref 66)
The harmonic perturbations (L)	10-28 mJ/m^2	(Ref 26)
Equilibrium melting point of Al-3 wt% Si (T_e)	851 K	(Ref 64)
Primary dendrite-calibrating factor (a_1)	250	(Ref 28)
Characteristic parameter ($G_o\epsilon$)	600×6 K/cm	(Ref 28)
Secondary dendrite-calibrating factor (a_2)	9	(Ref 28)

Acknowledgments

This project was supported by State Planning Organisation of Turkey (2003K 120880-4). The authors would like to thank the State Planning Organisation of Turkey for their financial support.

References

1. E.L. Rooy, *Metals Handbook*, Vol. 15, ASM International, Materials Park, Ohio, 1988, p 743–770
2. R. Trivedi and W. Kurz, Dendritic Growth, *Int. Mat. Rev.*, 1994, **39**(2) p 49–74
3. M.E. Glicksman and M.B. Koss, Dendritic Growth Velocities in Microgravity, *Phys. Rev. Let.*, 1994, **73**(4) p 573–576
4. D.P. Woodruff, *The Solid-Liquid Interface*, Cambridge University Press, London, 1973, p 80–84
5. J.A.E. Bell and W.C. Winegard, Dendrite Spacing in Tin-Lead Alloys, *J. Inst. Met.*, 1963, **93**, p 357–359
6. S.H. Han and R. Trivedi, Primary Spacing Selection in Directionally Solidified Alloys, *Acta Metall.*, 1994, **42**, p 25–41
7. W.W. Mullins and R.F. Sekerka, Morphological Stability of a Particle Growing by Diffusion or Heat Flow, *J. Appl. Phys.*, 1963, **34**, p 323–329
8. G.L. Ding, W. Huang, X. Lin, and Y. Zhou, Prediction of Average Spacing for Constrained Cellular/Dendritic Growth, *J. Cryst. Growth*, 1997, **177**, p 281–288
9. J.A. Warren and J.S. Langer, Prediction of Dendritic Spacings in a Directional-Solidification Experiment, *Phys. Rev. E*, 1993, **47**, p 2702–2712
10. L. Makkonen, Spacing in Solidification of Dendritic Arrays, *J. Cryst. Growth*, 2000, **208**, p 772–778
11. E. Çadırlı, I. Karaca, H. Kaya, and N. Maraslı, Effect of Growth Rate and Composition on the Primary Spacing, the Dendrite Tip Radius and Mushy Zone Depth in the Directionally Solidified Succinonitrile-Salol Alloys, *J. Cryst. Growth*, 2003, **255**, p 190–203
12. E. Çadırlı, N. Maraslı, B. Bayender, and M. Gündüz, Investigation of the Structure Parameters According to the Solidification Parameters for Pivalic Acid, *J. Mat. Sci.*, 1999, **34**, p 5533–5541
13. E. Çadırlı, N. Maraslı, B. Bayender, and M. Gündüz, Dependency of the Microstructure Parameters on the Solidification Parameters for Camphene, *Mat. Res. Bull.*, 2000, **35**, p 985–995
14. E. Çadırlı and M. Gündüz, The Directional Solidification of Pb-Sn Alloys, *J. Mat. Sci.*, 2000, **35**, p 3837–3848
15. M. Gündüz and E. Çadırlı, Directional Solidification of Aluminium-Copper Alloys, *Mat. Sci. Eng. A*, 2002, **327**, p 167–185
16. H. Kaya, E. Çadırlı, K. Keslioğlu, and N. Maraslı, Dependency of the Dendritic Arm Spacings and Tip Radius on the Growth Rate and Composition in the Directionally Solidified Succinonitrile-Carbon Tetrabromide Alloys, *J. Cryst. Growth*, 2005, **276**, p 583–593
17. S.Z. Lu and J.D. Hunt, A Numerical Analysis of Dendritic and Cellular Array Growth: The Spacing Adjustment Mechanisms, *J. Cryst. Growth*, 1992, **123**, p 17–34
18. J.D. Hunt, A Numerical Analysis of Dendritic and Cellular Growth of a Pure Material Investigating the Transition from Array to Isolated Growth, *Acta Metall.*, 1991, **39**, p 2117–2133
19. S.Z. Lu and J.D. Hunt, Numerical Modelling of Cellular and Dendritic Array Growth: Spacing and Structure Predictions, *Mat. Sci. Eng. A*, 1993, **173**, p 79–83
20. S.Z. Lu and J.D. Hunt, Numerical Modeling Dendritic Array Growth: Spacing and Structure Predictions, *Met. Trans. A*, 1996, **27A**, p 611–623
21. M.H. Burden and J.D. Hunt, Cellular and Dendritc Growth II, *J. Cryst. Growth*, 1974, **22**, p 109–116
22. J.S. Langer and H. Müller-Krumbhaar, Theory of Dendritic Growth-I. Elements of a Stability Analysis, *Acta Metall.*, 1978, **26**, p 1681–1687
23. V. Laxmanan, Dendritic Solidification-I. Analysis of Current Theories and Models, *Acta Metall.*, 1985, **33**, p 1023–1035
24. J.D. Hunt, *Solidification and Casting of Metals*, The Metal Society, London, 1979, p 3–9
25. W. Kurz and D.J. Fisher, Dendritic Growth and Limit of Stability Tip Radius and Spacing, *Acta Metall.*, 1981, **29**, p 11–20
26. R. Trivedi, Interdendritic Spacing: Part II. A Comparison of Theory and Experiment, *Met. Trans.*, 1984, **15A**, p 977–982
27. D. Bouchard and J.S. Kirkaldy, Scaling of Intragranular Dendritic Microstructure in Ingot Solidification, *Metall. Mater. Trans.*, 1996, **27B**, p 101–113
28. D. Bouchard and J.S. Kirkaldy, Prediction of Dendrite Arm Spacings in Unsteady- and Steady-State Heat Flow of Unidirectionally Solidified Binary Alloys, *Metall. Mater. Trans.*, 1997, **28B**, p 651–663
29. R. Trivedi and K. Somboonsuk, Constrained Dendritic Growth and Spacing, *Mater. Sci. Eng.*, 1984, **65**, p 65–74
30. J.W. Rutter and B.A. Chalmers, Prismatic Substructure Formed During Solidification of Metals, *Can. J. Phys.*, 1953, **31**, p 15–39

31. W.A. Tiller, K.A. Jackson, J.W. Rutter, and B. Chalmers, The Redistribution of Solute Atoms During the Solidification of Metals, *Acta Metall.*, 1953, **1**, p 428–437
32. Y. Miyata, T. Suzuki, and I.J. Uno, Cellular and Dendritic Growth, *Met. Trans.*, 1985, **16A**, p 1799–1805
33. J.T. Mason, J.D. Verhoeven, and R. Trivedi, Primary Dendrite Spacing: I Experimental Studies, *J. Cryst. Growth*, 1982, **59**, p 516–524
34. J.A. Spittle and D.M. Lloyd, *Solidification and Casting of Metals*, The Metals Society, London, 1979, p 15–20
35. R.A. Pratt and R.N. Grugel, Microstructural Response to Controlled Accelerations During the Directional Solidification of Al-6 wt % Si Alloys, *Mat. Char.*, 1993, **31**, p 225–231
36. A. Geying and L. Liu, Dendrite Spacing in Unidirectionally Solidified Al-Cu Alloy, *J. Cryst. Growth*, 1987, **80**, p 383–392
37. H. Jacobi and K. Schwerdtfeger, Dendrite Morphology of Steady State Unidirectionally Solidified Steel, *Met. Trans.*, 1976, **7A**, p 811–829
38. D. Liang, W. Jie, and H. Jones, The Effect of Growth Velocity on Primary Spacing of Al_3 Fe Dendrites in Hypereutectic Al-Fe Alloys, *J. Cryst. Growth*, 1994, **135**, p 561–564
39. M.A. Taha, Influence of Solidification Parameters on Dendrite Arm Spacings in Low Carbon Steels, *J. Mater. Sci. Lett.*, 1986, **5**, p 307–310
40. M.D. Peres, C.A. Siqueira, and A. Garcia, Macrostructural and Microstructural Development in Al-Si Alloys Directionally Solidified Under Unsteady-State Conditions, *J. Alloys Comp.*, 2004, **381**, p 168–181
41. R. Alberny, J. Serra, and M. Turpin, Use of Covariograms for Dendrite Arm Spacings Measurements, *Trans. Met. Soc. AIME*, 1969, **245**, p 55–59
42. D.G McCartney and J.D. Hunt, Measurement of Cell and Primary Dendrite Arm Spacings in Directionally Solidified Aluminium Alloys, *Acta Metall.*, 1981, **29A**, p 1851–1863
43. M.D. Dupough, D. Camel, and J.J. Favier, Natural Convective Effects in Directional Dendritic Solidification of Binary Metallic Alloys; Dendritic Array Primary Spacing, *Acta Metall.*, 1992, **40**(7), p 1791–1801
44. V.A. Wills and D.G. McCartney, A Comparative Study of Solidification Features in Nickel- Base Super Alloys: Microstructural Evolution and Microsegregation, *Mat. Sci. Eng.*, 1991, **415A**, p 223–232
45. M. Vijayakamur, S.N. Tewari, J.E. Lee, and P.A. Curreri, Dendrite Spacings in Directionally Solidified Super Alloy PWA-1480, *Mat. Sci and Eng.*, 1991, **132A**, p 195–201
46. S.N. Tewari and R. Shah, Macro Segregation During Steady-State Arrayed Growth of Dendrites in Directionally Solidified Pb-Sn Alloys, *Met. Trans.*, 1992, **23A**, p 3383–3392
47. K. Somboonsuk, J.T. Mason, and R. Trivedi, Inter Dendritic Spacings; Part I: Experimental Studies, *Met. Trans.*, 1984, **15A**, p 967–975
48. J.E. Spinelli, D.M. Rosa, I.L. Ferreira, and A. Garcia, Influence of Melt Convection on Dendritic Spacings of Downward, Unsteady-State Directionally Solidified Al-Cu Alloys, *Mat. Sci. Eng.*, 2004, **383A**, p 271–282
49. J. Lapin, A. Klimova, R. Velisek, and M. Kursa, Directional Solidification of Ni-Al-Cr-Fr Alloy, *Scripta Mat.*, 1997, **37**, p 85–91
50. R.M. Sharp and A. Hellawell, Solute Distributions at Non-Planar Solid-Liquid Growth Fronts-I Steady-State Conditions, *J. Cryst. Growth*, 1970, **6**, p 253–260
51. C.T. Rios and R. Caram, Primary Dendrite Spacing as a Function of Directional Solidification Parameters in an AI-Si-Cu Alloy, *J. Cryst. Growth*, 1997, **174**, p 65–69
52. J.E. Spinelli, I.L. Ferreira, and A. Garcia, Influence of Melt Convection on the Columnar to Equiaxed Transition and Microstructure of Downward Unsteady-State Directionally Solidified Sn-Pb Alloys, *J. Alloys Comp.*, 2004, **384**, p 217–226
53. J.E. Spinelli, M.D. Peres, and A. Garcia, Thermosolutal Convective Effects on Dendritic Array Spacings in Downward Transient Directional Solidification of Al-Si Alloys, *J. Alloys Comp.*, 2005, **403**, p 228–238
54. M. Gündüz, The Measurement of the Solid-Liquid Surface Energy, Ph.D. Thesis, Oxford University, 1984, p 60
55. D.G. McCartney, Studies on Cellular and Dendritic Solidification, Ph.D. Thesis, Oxford University, 1981, p 95
56. S. Ganesan, C.L. Chan, and D.R. Poirier, Permeability for Flow Parallel to Primary Arms, *Mater. Sci. Eng.*, 1992, **151A**, p 97–105
57. M.S. Bhat, D.R. Poirier, and J.C. Heinrich, Permeability for Cross Flow Through Columnar-Dendritic Alloys, *Metall. Trans.*, 1995, **26B**, p 1049–1056
58. V. Seetharaman, L.M. Fabietti, and R. Trivedi, Dendritic Growth in the Carbon Tetra Bromide and Hexachlorethane System, *Met. Trans.*, 1989, **20**, p 2567–2570
59. R. Trivedi and J.T. Mason, The Effect of Interface Attachment Kinetics on Solidification Interface Morphologies, *Met. Trans.*, 1991, **22A**, p 235–249
60. H. Honjo and Y. Sawada, Quantitative Measurements on the Morphology of a NH_4Br Dendritic Crystal Growth in a Capillary, *J. Cryst. Growth*, 1982, **58**, p 297–303
61. S. Liu, S.Z. Lu, and A. Hellawell, Dendritic Array Growth in the Systems NH_4Cl-H_2O and $[CH_2\ CN]_2$-H_2O: The Detachment of Dendrite Side Arms Induced by Deceleration, *J. Cryst. Growth*, 2002, **234**, p 740–750
62. G. Hansen, S. Liu, S.Z. Lu, and A. Hellawell, Dendritic Array Growth in the Systems NH_4Cl H_2O and $[CH_2\ CN]_2$-H_2O: Steady State Measurements and Analysis, *J. Cryst. Growth*, 2002, **234**, p 731–739
63. S.C. Huang and M.E. Glicksman, Fundamentals of Dendritic Solidification-I. Steady-State Tip Growth, *Acta Metall.*, 1981, **29**, p 717–734
64. T. Lyman, Ed., *Metals Handbook (Fractograph and Atlas of Fractographs)*, 8th Edition, Vol. 8, American Society for Metals (ASM Handbook Comittee), Metals Park, Ohio, 1973, p 263
65. P. Magnin, J.T. Mason, and R. Trivedi, Growth of Irregular Eutectics and the Al-Si System, *Acta Metall. Mater.*, 1991, **39**, p 469–480
66. M. Gündüz and J.D. Hunt, The Measurement of Solid-Liquid Surface Energy in the Al-Cu, Al-Si and Pb-Sn System, *Acta Metall.*, 1985, **33**, p 1651–1672